Structure, Deformation, and Failure of Flow-Oriented Semicrystalline Polymers

B. A. G. Schrauwen, L. C. A. v. Breemen, A. B. Spoelstra, L. E. Govaert,* G. W. M. Peters, and H. E. H. Meijer

Dutch Polymer Institute (DPI), Section Materials Technology (MaTe), Eindhoven University of Technology, P.O. box 513, NL-5600MB, Eindhoven, The Netherlands

Received June 7, 2004; Revised Manuscript Received September 1, 2004

ABSTRACT: This study deals with the influence of processing induced crystalline orientation on the macroscopic deformation and failure behavior of thin samples of polyethylene and polypropylene. Distribution and structure of flow-induced orientations were characterized by optical microscopy, X-ray diffraction techniques, and transmission electron microscopy. Hermans' orientation functions were either determined from the flat plate wide-angle X-ray diffraction patterns or calculated from full pole figures. The deformation behavior of the oriented samples was studied in both impact and tensile testing conditions and was found to be strongly anisotropic and related to the oriented structure. For all polymers studied, an increase of extended chains (shish) in the loading direction is proposed to cause an increase in the yield stress, and a lamellar structure oriented perpendicular to loading direction leads to an increase in strain hardening. In the extruded samples, where a low level of extended chains and a high level of oriented lamellae were found, the resulting combination of yield stress and strain hardening leads to homogeneous deformation. Brittle−ductile transitions in impact toughness of the molded samples could also be explained from differences in yield stress and strain hardening. Toughness enhancement was found to be most efficient with increasing strain hardening, and the effect was less pronounced in the polypropylene samples.

Introduction

Semicrystalline polymeric products are often manufactured from the molten state, using common processing operations, such as injection-molding or film and sheet extrusion. Within these processes, the molten polymer is subjected to shear and elongational flow, prior to crystallization. The resulting morphology can be quite different from what is observed under quiescent crystallization conditions. Typically oriented crystallite structures like "shish-kebabs" or lamellae row structures are formed if flow and cooling rates are large enough. This is generally the case near the cold walls of the injection mold, sheet extrusion chill rolls, and in thin extruded films.

Studies on injection-molding samples of various semicrystalline polymers, such as PP,[1−8] PE,[9] PAEK,[10,11] SPS,[12] and PEN,[13] show a clear multiphase structure of skin layers and a core when its cross section is observed with a polarizing microscope. The morphology of these "skin layers" varies with polymer melt properties and molding conditions,[1−5] but also along the flow path of the molded parts.[2,4,5,10−14] It is clear that the inhomogeneity of such samples affects physical properties like e.g. dimension stability,[14,15] Young's modulus, and tensile strength.[16−18]

Zuidema et al.[14,15] studied the dimensional stability of injection-molded polypropylene and found, in agreement with experimental observations, by numerical modeling that the thickness of the oriented layer decreases with distance from the injection gate, resulting in a different shrinking behavior. In the line with that work, Peters et al.[19] used numerical modeling with the goal to predict the spatial distribution of spherulites and oriented textures in controlled elongational flows. To complete their model, it should be expanded to distinguish between flow induced line nucleation and flow-induced point nucleation. The resulting difference in these two nucleation types is observed in the oriented layer, which generally consists of a part which is nucleated and crystallized in flow, the "shear layer", and a part which is only nucleated in flow, known as the "fine grained layer".[20] Besides the differences of these structures, the level of shear can also affect the resulting structure, e.g., row structures vs shish-kebabs in polyethylene.[21] For this reason it is important to clarify the structure of this layer in detail.

In this study we will focus on the influence of orientation on the mechanical behavior using conventional injection-molding and extrusion techniques to create the oriented structures. A low amount of orientation, often present in thick molded samples, does not have a significant effect on the mechanical behavior.[9] However, if oriented structures percolate through the sample, like observed in thin injection-molded samples,[22,23] extrusion films,[24] and certain hard filler modified injection-molded samples,[9] the anisotropic nature dominates mechanical properties, e.g., tensile and impact behavior. For this reason, in the literature, push−pull and shear-controlled orientation injection-molding (SCORIM) techniques are used to create a higher degree of orientation and an increase in oriented skin layer thickness in order to enhance the mechanical properties.[17,18,22−26] Most studies concerning the deformation behavior of flow-induced oriented semicrystalline polymers restrict to Young's modulus and tensile strength,[16−18,25] and only a few focus on the post yield or impact failure behavior.[1,22,27]

Structure−properties relationships can only be investigated if a detailed measurement of the distribution of the oriented structures is available, and most studies

* Corresponding author. E-mail: L.E.Govaert@tue.nl.

10.1021/ma048884k CCC: $27.50
Published on Web 10/19/2004

Table 1. Polymer Grades Used

material	trade name	M_w [g mol^{-1}]	M_n [g mol^{-1}]
PE-I	Stamylan HD 9089S	70 000	11 000
PE-E	Stamylan HD 8621	210 000	7 000
PP-I	Stamylan P 15M10	350 000	64 000
PP-E	Stamylan P 13E10	500 000	84 000

use X-ray scattering techniques in finding process−structure relations.[4−8,10−13,28−31] These orientation measurement techniques often require cumbersome cutting procedures. Some direct scanning measurements along the thickness direction in injection-molded parts are reported with birefringence,[31−33] Fourier transform infrared microscopy,[34,35] and wide-angle X-ray scattering techniques.[4,5] Although common processing techniques are not the optimal sample preparation methods to study the relationship between oriented structure and deformation, since the polymer experiences a complicated thermal and flow history, injection and extrusion techniques were used in this study to reconcile the deformation and failure behavior to oriented structures. A detailed measurement of the created structure was performed by optical microscopy, X-ray scattering techniques, and transmission electron microscopy. Differences in oriented structures are related to the tensile and impact toughness behavior, measured in flow and perpendicular to flow direction, using the correlation of yield, strain hardening, and "natural draw ratio", since these are considered to be the intrinsic properties determining the deformation and failure behavior.[36]

Experimental Section

Materials. The polymers used are an injection-molding and extrusion grade of high-density polyethylene (HDPE) and polypropylene (PP), all supplied by DSM, The Netherlands. In the following, these materials will be abbreviated as PE-I and PE-E for the injection-molding and extrusion grade of polyethylene, respectively, and PP-I and PP-E in the case of the polypropylenes. Table 1 summarizes the type of polymer grades used and their molecular weight. All data were provided by the supplier.

Injection-Molding. Rectangular plates, with dimension 70 × 70 × 1 mm^3, were injection-molded on an Arburg 320S/Allrounder 500-150 injection-molding machine. The mold was manufactured by Axxicon Moulds B.V. (Helmond, The Netherlands) and had a V-shaped runner of 5 mm thickness and an entrance of 70 × 1 mm^2, which is similar to the cross section of the plate cavity. The V-shaped runner caused the material to flow uniformly along the width of the cavity, which was proved by several short shot experiments. The amount of flow-induced orientation was varied by applying two extremes in injection-molding temperature (150 and 250 °C for PE-I and 185 and 260 °C for PP-I) and initial flow rate (10 and 100 cm^3/s). The extrusion grade of polyethylene, PE-E, was also used for injection-molding. Since the viscosity of this material is higher, injection temperature and flow rate were set to 250 °C and 10 cm^3/s, respectively. Mold cavity temperature was kept constant at 20 °C, and holding pressure was 600/400/200 bar for 1/2/5 s, respectively, giving a total packing time of 8 s. Filling time was obtained from the measured pressure profile in the nozzle, which had a diameter of 3 mm. Table 2 gives all variable molding conditions of the samples produced.

For tensile and impact specimens rectangular bars, with dimensions respectively 70 × 10 × 1 and 70 × 12.5 × 1 mm^3, were cut in flow and perpendicular to flow direction. The specimens perpendicular to flow direction were numbered according to their position from the cavity entrance as PERP-1, PERP-2, and PERP-3 (see Figure 1). The specimens tested in flow direction are abbreviated as FLOW samples. Dumbbell-shaped tensile specimens were made according to ISO 527 type 1BA on a milling machine, and Izod impact specimens were notched according to the ASTM D-256 protocol with a notching device.

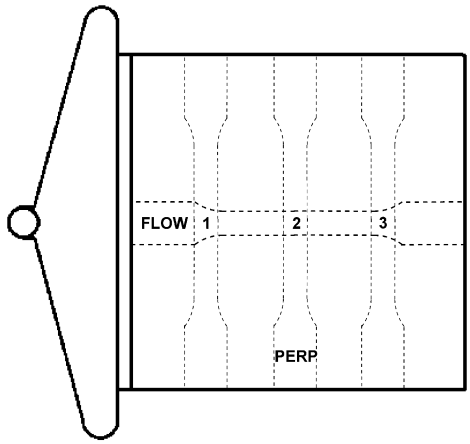

Figure 1. Schematic drawing of mold used for injection, including a V-shaped runner. Cutting positions for FLOW and PERP type of specimens are indicated.

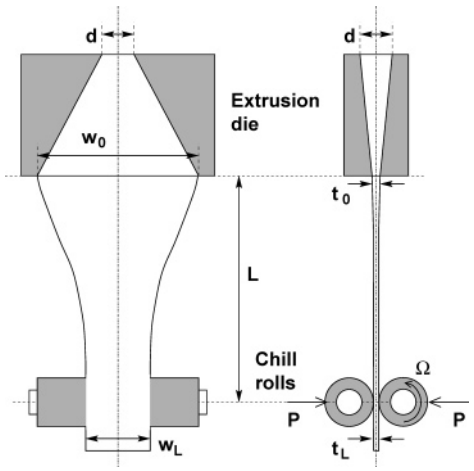

Figure 2. Schematic drawing of sheet extrusion die and chill rolls.

Table 2. Injection-Molding Codes and Conditions

code	melt temp [°C]	nominal flow rate [cm^3/s]	filling time [s]
PE-I A	150	10	1.6
PE-I B	150	80	0.2
PE-I C	250	10	1.6
PE-E	250	10	1.6
PP-I A	185	10	1.6
PP-I B	185	80	0.2
PP-I C	260	10	1.6

Extrusion Casting. Oriented polymer sheet samples were manufactured by film/sheet extrusion using the setup given in Figure 2. A Collin Teach-Line single screw extruder of 20 mm diameter operating at 130 rpm for PE-E and 110 rpm for PP-E was used to establish a constant flow rate of respectively 41.5 and 37.8 g/min. The polymer flow was stabilized in a channel of 15 × 15 mm^2 over a length of approximately 250 mm before entering the sheet extrusion die. Temperatures of extruder barrel, stabilization channel, and die were all set to 180 °C in the case of polyethylene and 220 °C in the case of polypropylene. The exit cross section, $t_0 \times w_0$, of the sheet die was set to 2.1 × 100 mm^2, and the distance from die to chill rolls, L, was approximately 150 mm. The chill rolls were water-cooled to 20 °C, and the thickness of the final polymer sheet was controlled by a gap opening, t_L, pressure, P, and speed, Ω, of the rolls.

During sheet extrusion, part of the polymer will be oriented by flow inside of the extrusion die, but most will be oriented

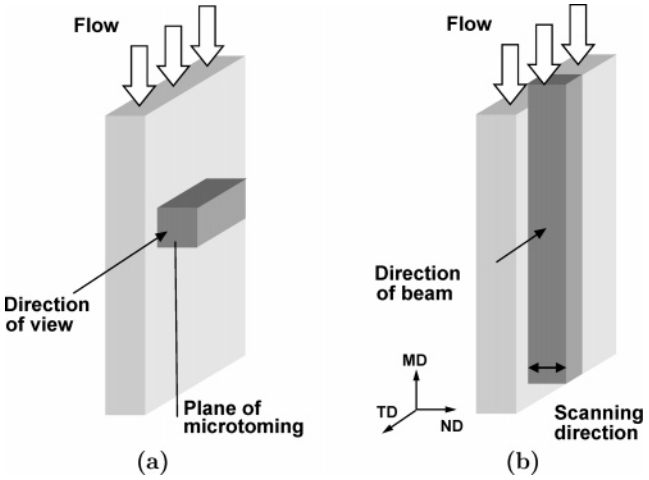

Figure 3. Illustration of injection-molded sample and direction of flow, view, and microtoming for TEM (a) and direction of flow, beam and scanning for WAXD (b).

Table 3. Extrusion Conditions

code	Ω [rpm]	P [bar]	w_L [mm]	t_L [mm]	DR = w_0t_0/w_Lt_L
PE-E 1	0.4	3	83	1	2.5
PE-E 2	0.8	3	61	0.65	5.3
PE-E 3	2.4	5	40	0.3	17.5
PP-E 1	0.2	1	100	1.8	1.2
PP-E 2	2.0	2	40	0.35	15

in the elongational flow due to drawing by the chill rolls. The speed of the rolls was varied, and the draw ratio was determined as the ratio of initial and final cross section of the sheets. Chill roll speed, pressure, and draw ratio of the different samples are given in Table 3. For tensile testing, specimens were cut from the center of the oriented sheets in extrusion direction using a dumbbell-shaped (ISO 527 type 1BA) cutting knife.

Microscopy. Two microscopic techniques were used to gain first insight in the oriented structure of the samples. Optical light microscopy (LM) was used to visualize the thickness of oriented skin layers. Cross sections of approximately 3−7 μm were prepared at low temperatures of approximately −130 °C, using liquid nitrogen, at a Reichert Ultracut E rotary microtome, equipped with a glass knife. The cross sections were viewed between crossed polars on an Axioplan imaging microscope and pictures were made with the combined Axio Cam camera.

Transmission electron microscopy (TEM) was used to visualize the crystal lamellae structure in the oriented and nonoriented parts of the samples. Samples were trimmed at low temperature (−130 °C) and subsequently treated for 20 h with a ruthenium tetraoxide (RuO_4) solution.[37] Ultrathin sections were obtained at room temperature using the microtome, equipped with a diamond knife. TEM was performed on a JEOL JEM 2000 FX microscope, operated at 80 kV. Figure 3a shows the direction of viewing and microtoming with respect to flow and sample thickness.

X-ray Diffraction. Flow-induced oriented structures in the molded samples were analyzed by recording 2D wide-angle X-ray diffraction (WAXD) film patterns. WAXD experiments were performed at the European Synchrotron Radiation Facilities (ESRF) in Grenoble (France) at the microfocus beamline (ID13). Since the initial beam size was 5 μm and the collimator-to-sample distance was about 3 mm, the resulting beam size transmitting through the sample (TD direction) is less than 10 μm, enabling us to examine the different structures over the thickness of the specimens. Samples of 1 mm width were cut from the middle of the specimens, and WAXD patterns were recorded with a 2D-MAR CCD detector (resolution: 2048 × 2048), scanning the sample with a moving stage over the thickness of the specimen (ND direction). Cutting, scanning, and beam direction are illustrated in Figure 3b. The exposure time was on the order of 1−5 s, using a X-ray wavelength of 0.975 Å and a sample-to-detector distance of 150 mm. Scanning was done with steps of 10 μm over half the thickness of the injection-molded samples (0.5 mm) and over the full thickness of the extruded sheets.

Since the resulting X-ray diffraction patterns of the extruded polyethylene samples showed an approximately uniform distribution of orientation over the sample thickness, these samples were used for creating pole figures. Similar samples as shown in Figure 3b were cut from the extruded sheets. The width of the samples was set equally to the sheet thickness, resulting in rectangular samples, reducing intensity differences due to path length variations. These samples were positioned on a goniometer with the rotation axis being in the middle of the ND−TD plane of the sample and rotated around the machine direction (MD) over 90°, collecting 2D WAXD patterns every 5°. Intensities of these collected patterns were taken every 5° over the azimuth angle of the 110, 200, and 020 Debye rings and used as input data to create full pole figures in the software program BEARTEX2000.[38]

Small-angle X-ray scattering (SAXS) patterns were taken at the high-brilliance beamline (ID2) at the ESRF, using a beam size of 300 × 300 μm, a wavelength of 0.995 Å, sample-to-detector distance of 10 m for polyethylene and 5 m for polypropylene samples, and a Frelon CCD camera (resolution: 1024 × 1024). The larger beam size is too large for accurate scanning over the sample thickness, and patterns are only collected with the beam transmitting through the complete sample in ND direction.

Mechanical Testing. Tensile tests on the dumbbell-shaped tensile specimens were performed on a Zwick Z010 tensile testing machine, at a constant speed of 5 mm/min, which corresponds to a constant initial strain rate of 1.5×10^{-3} s^{-1} for the applied clamp-to-clamp distance of 55 mm. Engineering stress−strains curves were constructed from the measured force, clamp displacement, and initial cross section of the specimens.

Impact tensile test were performed on the Izod impact bars at a speed of 1 m/s, using a Zwick Rel hydraulic tensile testing machine. To ensure the desired initial speed, a pick-up unit was used to allow the piston to accelerate before loading the specimen. To reduce dynamic effects, the contact area between the pick-up unit and the piston was damped by a rubber pad.[39] Piston displacement and force, using a piezoelectric force transducer, were measured at a sample rate of 2.5 MHz. The impact toughness energy was calculated by integration of the measured force−displacement curve, divided by the initial cross-sectional area behind the notch. All tests were performed at room temperature and in 5-fold.

Results and Discussion

Optical Microscopy. Injection-molded samples of semicrystalline polymers are known to show an inhomogeneous structure, over both the thickness as the length of the sample. Structure and thickness of the "skin layers" vary with the molding conditions applied: initial flow rate, melt, and mold temperature. Figure 4 shows optical micrographs of the complete cross section of sample PE-I A taken from a position close to the injection-molding gate (a), in the middle of the sample (b), and far from the gate (c), as illustrated in Figure 1. At all positions, several structural layers can be distinguished: a thin "skin layer" (A), a "transition layer" (B), a "shear layer" (C), a "fine-grained layer" (D), and an "isotropic core" (E). At the positions near the gate (a) and in the middle (b) the "shear layer" shows a very highly oriented "fiberlike layer" (F) which is partly delaminated upon microtoming. The total thickness of the oriented layers (A, B, C, F) is largest at the position close to the gate (a), on the order of 350 μm, decreases a to approximately 300 μm in the middle of the sample

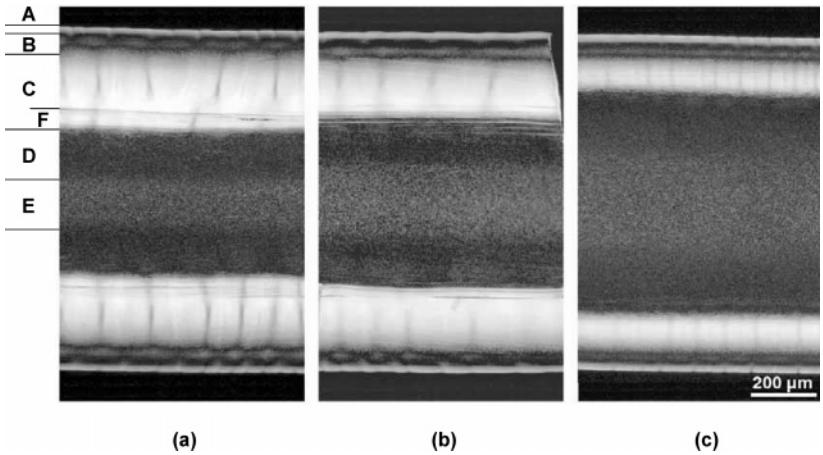

Figure 4. Optical micrographs of cross section of injection-molded sample of PE-I A at position close to the gate (a), mid of samples (b), and far from the gate (c) viewed between cross-polars at 45° with flow direction, showing difference in thickness of oriented skin layer. We distinguish the "skin layer" (A), "transition layer" (B), "shear layer" (C), "fine-grained layer" (D), "isotropic core" (E), and "fiberlike layer" (F).

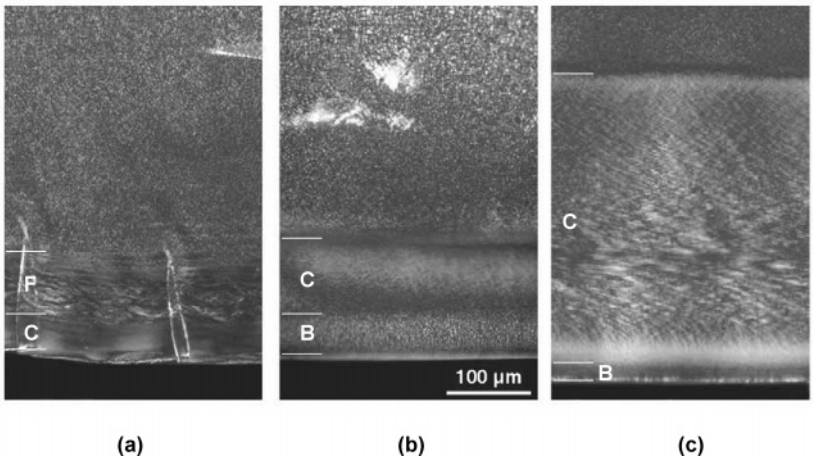

Figure 5. Optical micrographs of cross section of injection-molded samples PE-I B (a), PE-I C (b), and PE-E (c) (for coding see Table 2) viewed between cross-polars at 0° and 90° with flow direction, showing oriented skin layers.

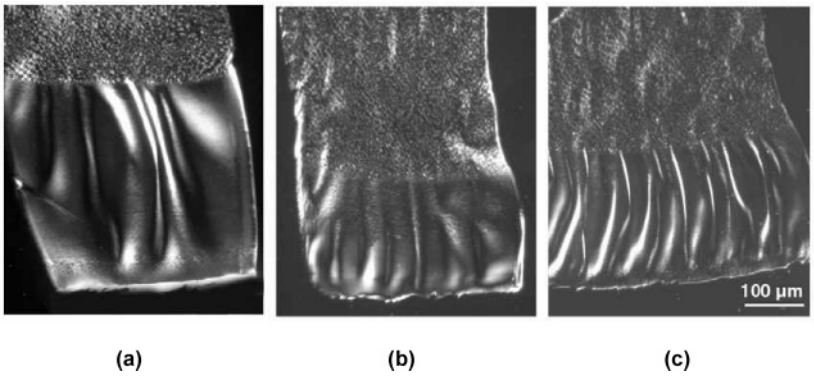

Figure 6. Optical micrographs of cross section of injection-molded PP-I samples A (a), B (b), and C (c) (for coding see Table 2) viewed between cross-polars at 0° and 90° with flow direction, showing oriented skin layer.

(b), and is clearly smallest at the end position (c), ≈200 μm.

Reduction of the oriented layers' thickness at increasing distances from the injection gate was observed for all injection-molded samples. However, the thickness of the oriented layers strongly depends on molecular weight and molding conditions applied as shown in Figures 5 and 6. Figure 5 shows optical micrographs of cross sections of the edge, taken from the middle of the samples, of the low molecular weight polyethylene samples PE-I B and PE-I C, which can be compared with the cross section of sample PE-I A, shown in Figure 4. For both the samples PE-I B and PE-I C, the total thickness of the oriented layer is found to be on the order of 150 μm, which is half the thickness observed in sample PE-I A. The higher flow rate applied in sample PE-I B increases the shear stresses in the polymer, and therefore orientation is expected to be larger. However, increasing the flow rate also decreases the filling time and, consequently, the time that the polymer melt experiences flow stresses. Moreover, orientation is strongest in the melt close to the penetrating

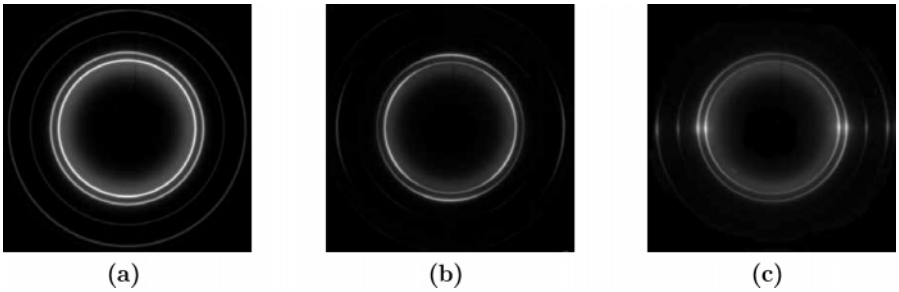

Figure 7. Typically recorded WAXD patterns of PE, taken in TD direction from the core (a) or from the skin (b, c) of injection-molded samples or from extrusion sheets (b, c).

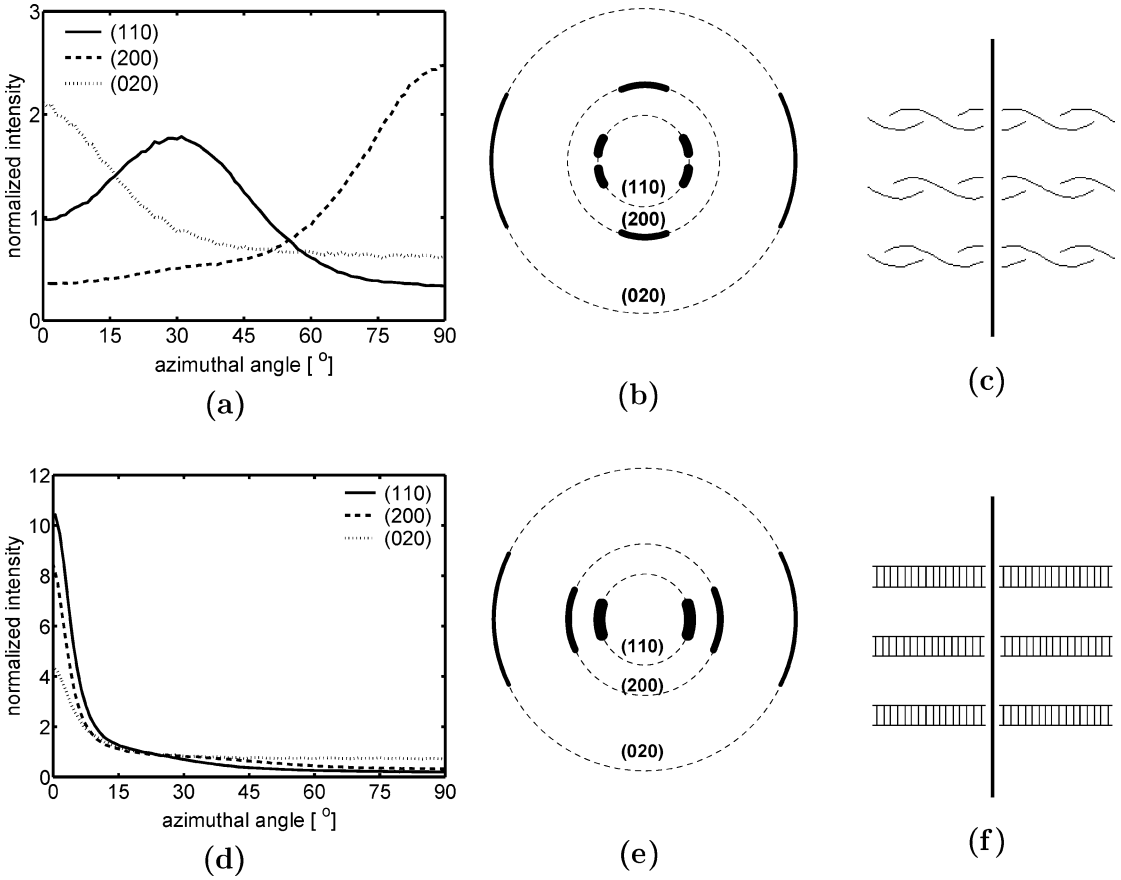

Figure 8. Normalized azimuthal intensity curves of (110), (200), and (020) reflections (a, d) indicating typical oriented WAXD patterns (b, c) of shish-kebab structures with twisted (c) and untwisted (f) lamellae, according to Keller and Machin.[21]

solidifying layer (initially this is the cavity wall), where the relaxation times grow high. With increasing filling time the range of this layer is extended and thus the oriented layer. What else can be observed in Figure 5 is that the distribution of the structural layers, as observed in Figure 4, is now different. The "transition layer" (B) has completely disappeared, whereas the "fiberlike layer" (F), showing delamination upon microtoming, is larger. This is indeed the result of the higher shear stresses near the mold cavity walls due to the higher flow rate. Increasing the melt temperature at similar flow rate (sample C) decreases the total oriented layer thickness at the cost of the higher oriented "shear layer" (C) and "fiberlike layer" (F). A higher melt temperature is accompanied by a lower melt viscosity, decreasing the resulting orientation in the polymer. The effect of melt viscosity is also observed when injection-molding the polyethylene extrusion grade (PE-E), resulting in a thick oriented skin layer as shown in Figure 5c. Since the melt viscosity of this grade is not in the range of conventional injection-molding grades, the melt temperature used to injection-mold this polymer was set at 250 °C, still giving a thick oriented skin layer.

Figure 6 shows the optical micrographs of half the cross section of the different injection conditions of the PP-I grade (A, B, C), all taken from the middle of the samples (position 2). Similar to polyethylene, the total oriented layer thickness is found to be largest for the low injection flow rate and low melt temperature (sample A), but a clear appearance of different orientation layers, like observed in polyethylene, is absent in polypropylene and only one thick oriented layer is observed. The reason for this can be due to a different position of the cross-polars, giving less brightening of the different oriented layers. A more detailed characterization will be given in the X-ray diffraction section, where also the level of orientation in the different layers is determined. Further results on structure and properties of both polymers are reported separately here for clarity of discussion.

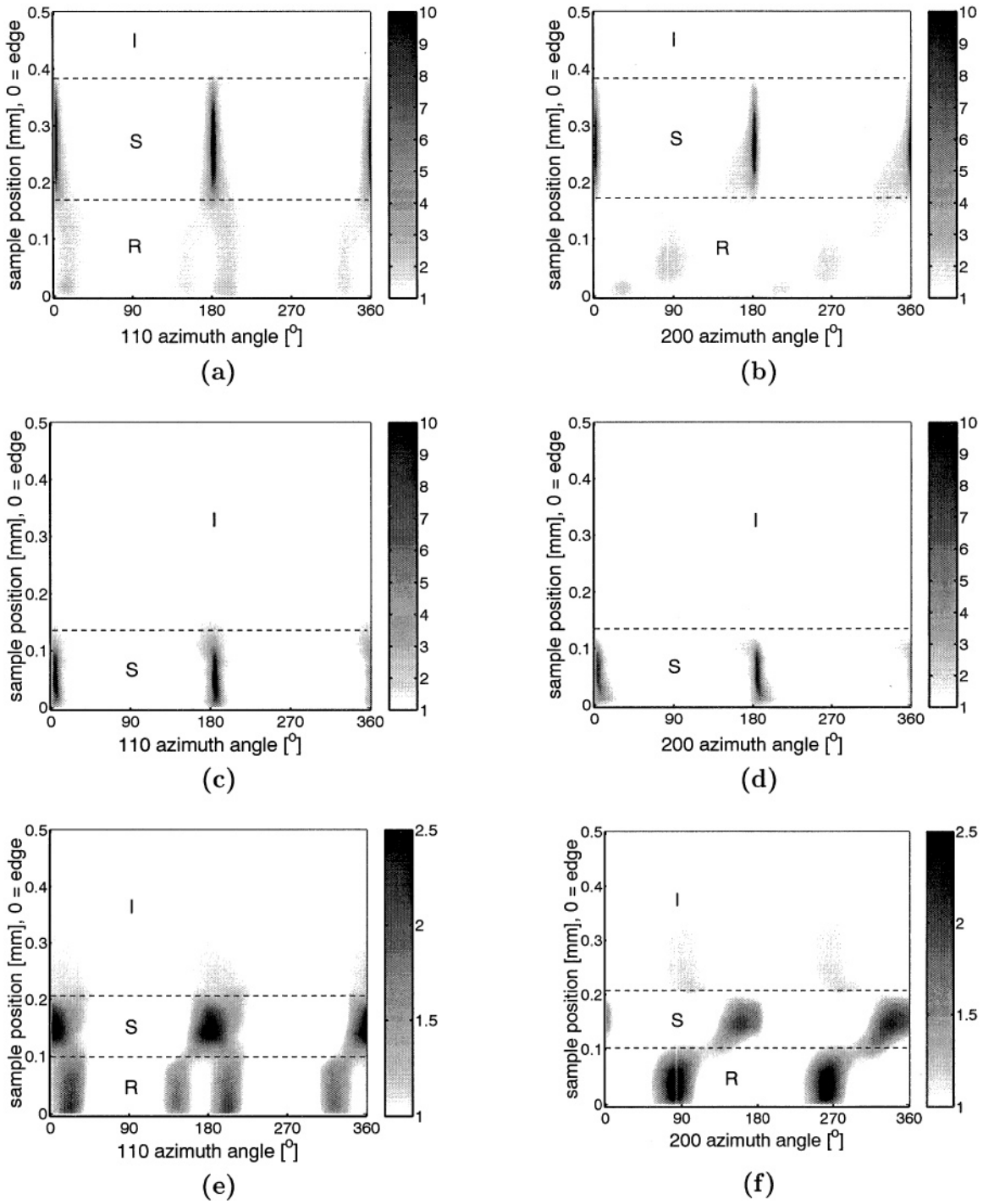

Figure 9. Normalized intensity at azimuthal angle of WAXD patterns scanned over half the thickness of samples: PE-I A (a, b), PE-I B (c, d), and PE-I C (e, f). A normalized intensity of 1 over the complete azimuthal scan represents an isotropic spherulitical structure (I), intensity variations indicate the presence of a Shish-kebab (S), or row (R) structure as indicated in Figure 8.

WAXD of Polyethylene. The 2D WAXD images recorded at the different sample thickness positions for the polyethylene samples typically show patterns as given in Figure 7. The first pattern, showing full Debye rings of (110), (200), and (020) reflection of the crystal lattice planes, was found in the core of the injection-molded samples. These patterns were nearly completely unoriented, which is consistent with the isotropic spherulitic structure of the polarized micrographs (Figures 4 and 5). The two oriented patterns shown are typical patterns taken from the extruded sheets or from the skin of injection-molded samples. Detailed intensity variation of the second pattern is difficult to observe since orientation is low. For this reason, (110), (200), and (020) reflections were isolated using the FIT2D data analysis software, and intensities of these reflections were normalized with the total intensity of each reflection and plotted against the azimuth angle from 0° to 90°, 0° being the equatorial (ND) direction (see Figure 8a,d). Keller and Machin[21] showed that the two typical patterns of oriented structure observed in polyethylene (Figures 7 and 8b,e) originate from shish-kebab structures.

In flow, the high end tail of the molecular weight distribution, which has the largest relaxation time, is able to orient into fibrous crystals acting as nucleating threads for the lower molecular weight part, which relax

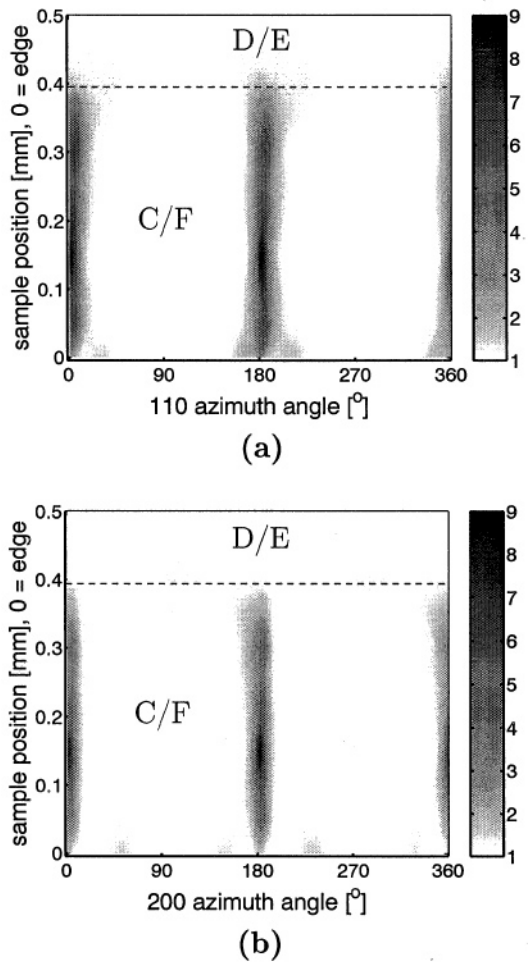

Figure 10. Normalized intensity at azimuthal angle of WAXD patterns scanned over half the thickness of samples: PE-E (a, b). A normalized intensity of 1 over the complete azimuthal scan represents an isotropic structure (I), intensity variations indicate the presence of a shish-kebab (S) structure as indicated in Figure 8.

much faster during and after flow. Lamellar overgrowth takes place on these oriented threads, resulting in a shish-kebab structure. The degree of stretch, caused by the strength of the flow, can affect not only the number of nucleating threads (shish) but also the configuration of the transversely growing lamellae (kebabs). In weaker orientating flows, fewer and hence more widely spaced shish are formed, and the transverse lamellae (kebabs) show twisting in growth direction due to chain tilting (Figure 8c), such as is usual in (polyethylene) spherulites. This twisted, oriented lamellae structure is better known as the so-called "row strucure", as observed in melt-extruded polyethylene films.[21] So higher stresses stimulate the formation of shish but also influence the lamellar development as they will be prevented from twisting (see Figure 8f).

The method of isolating the different reflections and normalizing the intensity of the WAXD patterns (Figure 8) is applied to all patterns collected from scanning over half the thickness of the samples. The advantage of normalization is that intensity differences, caused by variations in sample thickness, are circumvented, and comparison of different samples and positions can be made. Figure 9 shows the normalized intensity of the (110) and (200) reflections as a function of full azimuthal angle (0°−360°) and distance from the edge (0−0.5 mm) of the injection-molded lower molecular weight grade, PE-I. The results of the higher molecular weight grade, PE-E, are given in Figure 10. The core and skin layers are identified as follows: (I) the core is isotropic, showing no intensity variations over the azimuth angle, giving a normalized intensity of 1 over the complete azimuth angle; (S) strong oriented layers show intensity spots in both reflections at the equator, interpreted by fiber or shish-kebab structures where no lamellae twisting is present (Figure 8); (R) layer showing a row structure (twisted lamellae) of lower orientation, represented by splitting up of the (110) intensity spots and by (200) spots at the meridian. The distribution of the layers can be compared with the ones observed in the optical micrographs (Figures 4 and 5). Sample PE-I A, which is injection-molded at low temperature and flow rate, shows the largest total oriented layer. Orientation starts with a lower oriented row structure (R), which is visualized as the "transition layer" (B) in Figure 4, and increases at further distance of the edge forming an untwisted shish-kebab or fiber structure (S), which is visualized as the "shear layer" (C) in Figure 4. The reason for an increase in orientation for positions further from the edge is that solidification of the polymer at the edge forms a new wall where shear rate is increased due to a decrease in cross-sectional area of the cavity.

Increasing the initial flow rate (sample PE-I B) is accompanied by higher shear stresses at the cavity wall, resulting in the formation of a highly oriented shish-kebab structure directly near the wall. Lower oriented row structures are absent, which was illustrated by the disappearance of the "transition layer" (B) in Figure 5a. The oriented layer thickness decreases due to the shorter filling time combined with the limited cooling of the polymer. Increasing the temperature (sample PE-I C) gives a similar distribution of a lamellae row layer ("transition layer") and shish-kebab ("shear layer") as seen in sample PE-I A, but with a decreased thickness and orientation level, since crystallization rate and stresses are lower in the polymer melt. Injection-molding of the higher molecular weight, PE-E, gives a thick layer of highly oriented structure (S) (Figure 10). Both viscosity and long end tail, promoting the formation of shish, are responsible for this.

Comparison of the layer thickness observed in Figures 4 and 5 with that of Figures 9 and 10 indicates a thicker layer in some samples observed by X-ray scanning. However, a slightly rotational tilt along the MD direction of the sample when mounted in the X-ray diffraction setup can be the reason for this since the sample dimensions used were relatively large (1 mm). Using a smaller length through which the beam is transmitted would probably give more reliable results. Furthermore, the "skin layer" (A) observed at the edge in the optical micrographs is difficult to measure with the X-ray diffraction technique since scattering on the sample edge disturbs the quality of WAXD images and were therefore not used. The results of X-ray scanning along the thickness of the extruded sheets of PE-E are not given here. These samples showed a similar level of orientation over the full thickness and were consequently used to create pole figures, discussed later in this study.

TEM of Polyethylene. Figure 8 proves that WAXD analysis is capable to distinguish between twisted "row structures" and nontwisted "shish-kebab"-like structures. However, the highly oriented WAXD pattern

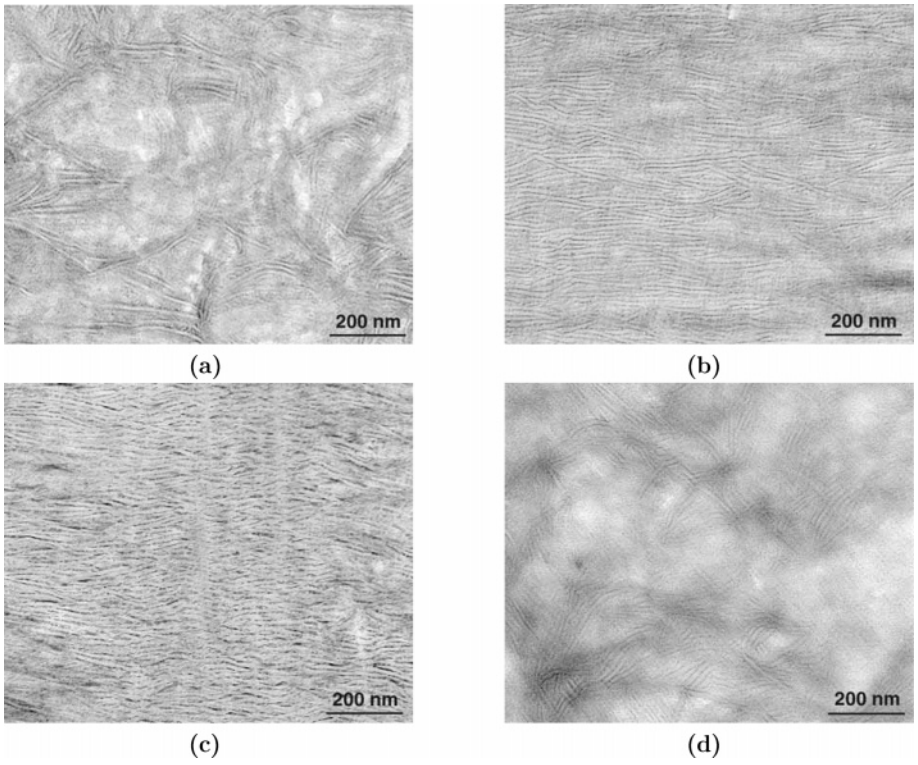

Figure 11. Transmission electron micrographs of injection-molded sample PE-I showing (a) low oriented row structure in the "transition layer", (b) highly oriented row structure in the "shear layer", (c) shish-kebab structure in layer F of "shear layer", and (d) isotropic structure in the core. Flow is in vertical direction of images.

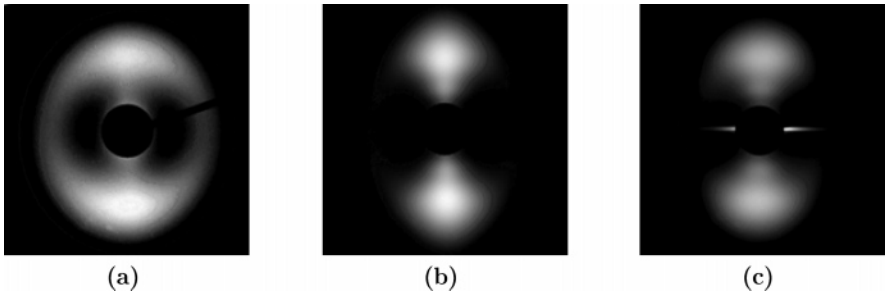

Figure 12. SAXS patterns of extruded PE-E samples, PE-E 1 (a) and PE-E 3 (b) and injection-molded PE-E sample (c) taken in ND direction with the beam going through the complete thickness. Flow is in vertical direction of images.

shown for the nontwisted structures (Figure 8d,e) is similar to patterns from PE fibers. The presence of the "fiberlike layer" (F), as observed with the delaminated area in the optical micrographs, within the "shear layer" (C) is not directly distinguished from the other layers in the WAXD results. Hence, a more detailed investigation is carried out.

Figure 11 gives transmission electron micrographs taken at different positions in the cross section of sample PE-I A. The first image is taken from the "transition layer" (B), which is expected to have a row structure. Although a clear row oriented structure is not observed, the majority of the lamellae indeed show a preferential alignment perpendicular to flow (flow is in vertical direction). Part of the lamellae, that are twisted, are viewed in plane direction and are not seen in this transmission mode. The second image shows a clear oriented lamellae structure taken from the "shear layer" (C). Here, the lamellae are not twisted and are all viewed in cross-sectional area. The third image is taken from the "fiberlike layer" (F) and again shows a high orientation of lamellae. However, the lengths of the lamellae are shorter than in the previous image, and even shishlike patterns are visible. The majority of the polymer is, however, still present in lamellae, so the term "fiberlike layer", used so far, should be reconsidered not to indicate a fiber texture. The last image is taken from the core of the sample, showing a random arrangement of lamellae.

The image in Figure 11a is also typical for the structure found in the extruded samples. More convincing evidence that this is a lamellae row structure will be given with the following results of small-angle X-ray scattering measurements.

SAXS of Polyethylene. Since small-angle X-ray scattering images were collected at with a beam spot of 300×300 μm, and not with the microfocus beam, it is impossible to identify the different layers. Therefore, SAXS images were taken with the beam exposing the complete samples thickness in ND direction and therefore representing the average morphology of the samples. Most interesting is the morphology of the lowest and highest orientation levels as obtained from the WAXD measurements. Figure 12 gives, in order of increased orientation, the SAXS patterns of the extruded PE-E 1, PE-E 3, and injection-molded PE-E samples. All images

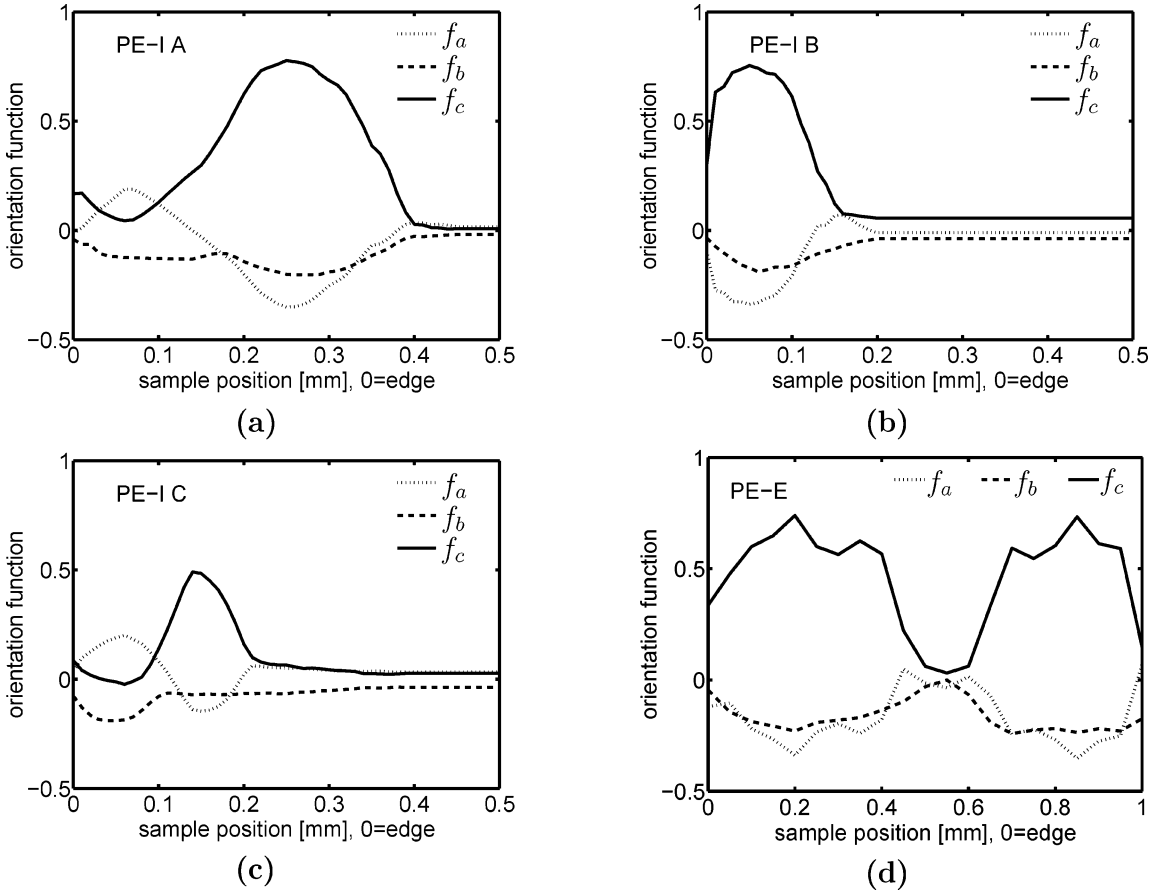

Figure 13. Orientation functions in flow (MD) direction over half the thickness of injection-molded samples of PE-I A (a), PE-I B (b), PE-I C (c), and full thickness of PE-E (d).

show spots at the meridian, originating from lamellae oriented perpendicular to the flow direction, which is vertical.

First of all, this proves the presence of a row structure in all extruded samples, which was difficult to interpret from the TEM images of these samples (Figure 11a), being more pronounced in the sample subjected to a larger draw ratio. Second, in the strongly oriented injection-molded samples the aligned lamellae are still present, indicating that the morphology is definitely not a full fiber texture. However, the strong intensity streak near the beam stop in equatorial direction is a result of the large number of shish present. Finally, the rain drop shape of the intensity spots indicates the variation in long spacing, which is known to be a result of the tapered shape and interlocking of the kebabs.[40,41]

Orientation Functions of Polyethylene. A quantitative measure of uniaxial orientation, such as present in fibers, can be formalized using the Hermans orientation factor (f_H). The orientation function is defined as

$$f_H = \frac{3\langle\cos^2\phi\rangle - 1}{2} \tag{1}$$

where ϕ is the angle between the unit within a crystal of interest (e.g., chain axis c) and a reference axis (e.g., fiber or machine direction).

$\langle\cos^2\phi\rangle$ is defined as

$$\langle\cos^2\phi\rangle = \frac{\int_0^{\pi/2} I(\phi)\cos^2\phi\sin\phi\,\mathrm{d}\phi}{\int_0^{\pi/2} I(\phi)\sin\phi\,\mathrm{d}\phi} \tag{2}$$

where $I(\phi)$ is the pole concentration representing the relative amount of crystalline material having plane normals in the direction of ϕ, ψ, such that

$$I(\phi) = \int_0^{2\pi} I(\phi,\psi)\,\mathrm{d}\psi \tag{3}$$

Regarding the orientation in the polyethylene samples, we are interested in the c-axis (chain) orientation in the direction of flow (MD). Assuming a rotational symmetry around the machine direction (fiber symmetry) and defining the angles δ, ϵ, and σ of respectively the a-, b-, and c-axis with the machine direction, the orientation functions are given by

$$f_a = \frac{3\langle\cos^2\delta\rangle - 1}{2} \tag{4}$$

$$f_b = \frac{3\langle\cos^2\epsilon\rangle - 1}{2} \tag{5}$$

$$f_c = \frac{3\langle\cos^2\sigma\rangle - 1}{2} \tag{6}$$

The a- and b-axis orientation (f_a, f_b) can be directly obtained from the measured (200) and (020) reflections, from

$$\langle\cos^2\delta\rangle = \langle\cos^2\phi_{200}\rangle \tag{7}$$

$$\langle\cos^2\epsilon\rangle = \langle\cos^2\phi_{020}\rangle \tag{8}$$

Without the pure reflections from the c-axis, Wilchin-

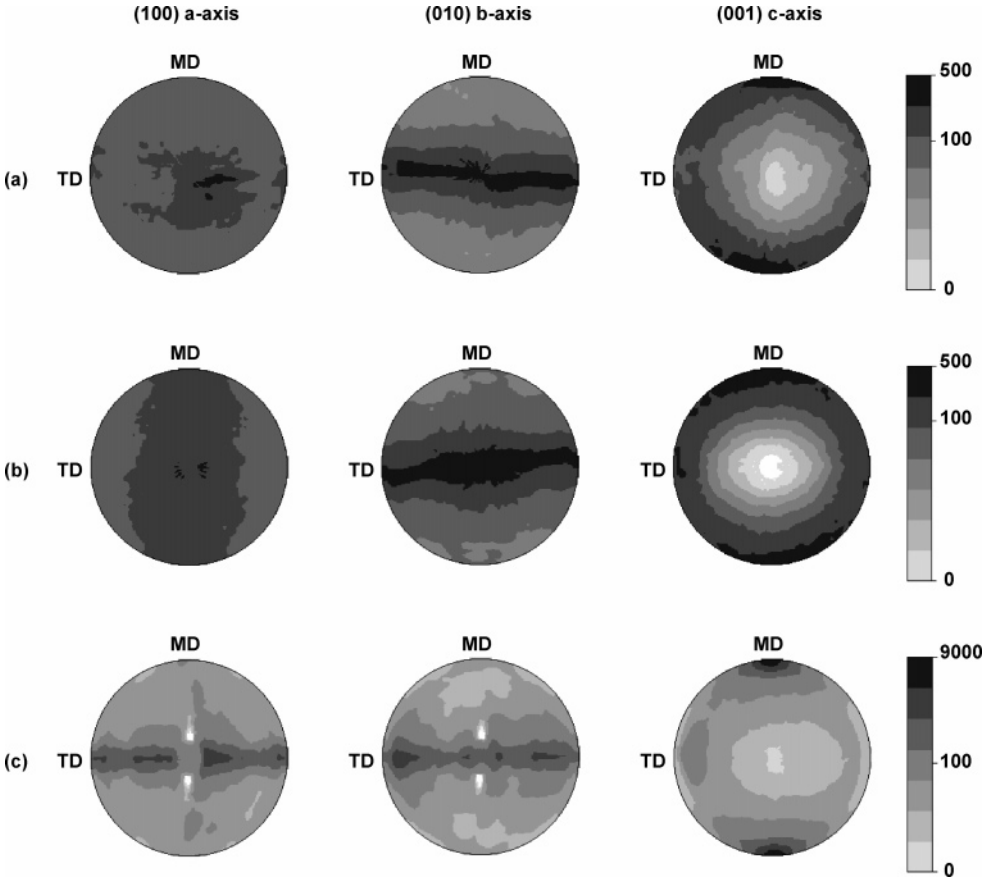

Figure 14. Pole figures of extruded samples PE-E 1 (a), PE-E 2 (b), and PE-E 3 (c). Intensity scale is logarithmic.

sky's method[42] is used to obtain information about the *c*-axis orientation:

$$\langle \cos^2 \sigma \rangle = 1 - 0.565\langle \cos^2 \phi_{200} \rangle - 1.435\langle \cos^2 \phi_{110} \rangle \quad (9)$$

where $\langle \cos^2 \sigma \rangle$ is calculated from the strong (110) and (200) reflections, using the angle between the normal of the (110) plane and the *a*-axis (56.6° for PE) and the orthogonality relationship in the orthorhombic crystal structure:

$$\langle \cos^2 \delta \rangle + \langle \cos^2 \epsilon \rangle + \langle \cos^2 \sigma \rangle = 1 \quad (10)$$

When chains are perfectly aligned along the reference axis, $f_c = 1$, whereas $f_c = -1/2$ for chains aligned perpendicular to the reference axis. For random orientation, $f_c = 0$.

Complete pole figures of the injection-molded samples were not measured, as this is useless since upon rotation of the sample uniqueness of the different layers is lost. Despite this, we will assume a complete rotational symmetry of each layer along the machine direction and, at the risk of oversimplification, use the measured 2D WAXD patterns to determine the crystalline orientation functions. Figure 13 gives the distribution in flow direction over half the thickness (full thickness for PE-E) of the samples, taken at position 2 (Figure 1). The distribution of the strongest oriented "shear layer" is observed with values of f_c of approximately 0.5 to 0.75, whereas the *b*-axis, representing the lamellar growth direction, inclines perpendicular to flow direction ($f_b < 0$). The core shows an isotropic morphology since all functions are zero, whereas the lower oriented "transition layer" does not show a clearly interpretable orientation distribution. The latter is due to the row structure of this layer, which is expected not to be of rotational symmetry, and thus determination of the Hermans orientation functions on results from single 2D WAXD images does not apply. Nevertheless, the average values of f_c over the sample thickness are given in Table 4.

Table 4. Average *c*-Axis Orientation Functions $f_{c,av}$

	Injection			
	PE-I A	PE-I B	PE-I C	PE-E
$f_{c,av}$	0.31	0.21	0.10	0.46
	Extrusion			
		PE-E 1	PE-E 2	PE-E 3
$f_{c,av}$		0.37	0.38	0.59

Lindenmeyer and Lustig[24] already pointed out that the technique of using flat plate X-ray diffraction photographs can lead to erroneous conclusions, at least in extruded polyethylene films, and emphasized the importance of pole figures. Since the extruded sheets showed similar orientation patterns along the complete sample thickness, these were used to create complete pole figures, which are presented in Figure 14. Pole figures of the three principal crystallographic directions are plotted: *a*-axis (100), *b*-axis (010), and *c*-axis (001).

The (010) pole figures of extruded sheets of low melt draw ratio (PE-E 1: DR = 2.5; PE-E 2: DR = 5.3) indicate that the *b*-axis is dispersed in the plane perpendicular to machine (flow) direction. The *c*-axis shows a small tendency toward MD direction but still shows a strong distribution around normal direction (ND). The *a*-axis is clearly uniformly dispersed in the plane of the sheet. These findings are in agreement with

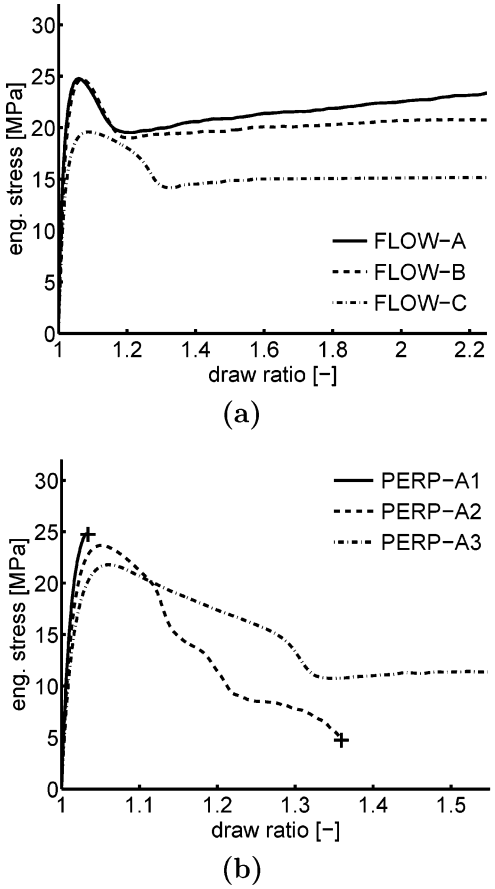

Figure 15. Macroscopic tensile behavior of injection-molded samples of PE-I A, PE-I B, and PE-I C, tested in flow direction (a) and sample PE-I A, tested perpendicular to flow direction (b) at different distances from the gate (1, 2, 3).

Table 5. Tensile and Impact Testing Results of Injection-Molded PE Specimens (− = Brittle Failure)

	σ_y [MPa]	λ_n	Izod [kJ/m^2]
		PE-I A	
FLOW	25	4.5−3.5	160
PERP-1	−	−	3.5
PERP-2	24	−	2.5
PERP-3	22	8	9
		PE-I B	
FLOW	25	5	35
PERP-1	22.5	7	10
PERP-2	22	7.5	40
PERP-3	21.5	8	50
		PE-I C	
FLOW	19.5	5	125
PERP-1	22	8.5	10
PERP-2	21.5	8	15
PERP-3	19.7	7.5	70
		PE-E	
FLOW	−	−	15
PERP-1	24.6	5.5	45
PERP-2	23.2	5.3	125
PERP-3	21.7	5	130

the row structure presented by Keller[21,41] since the *b*-axis is known to be the direction of radial growth, with the *a*- and *c*-axis tending to rotate around this growth direction (twisting of lamellae). When the melt draw ratio is drastically increased (PE-E 3: DR = 17.5), the *c*-axis shows the strongest orientation in the direction of flow, whereas both *a*- and *b*-axis are almost randomly dispersed in the plane perpendicular to MD (ND−TD plane). This indicates a rotational symmetry of orientation around MD and is consistent with a highly oriented nontwisted lamellae orientation perpendicular to flow direction. Caution should be taken regarding the intensity levels since the thickness of the samples is not constant, and rotation of the square samples causes both differences in effective volume and path length of the beam. Suitable corrections should be made if the intensities are to be compared. Finally, the average *c*-axis orientation function was calculated from the complete orientation distributions and summarized in Table 4.

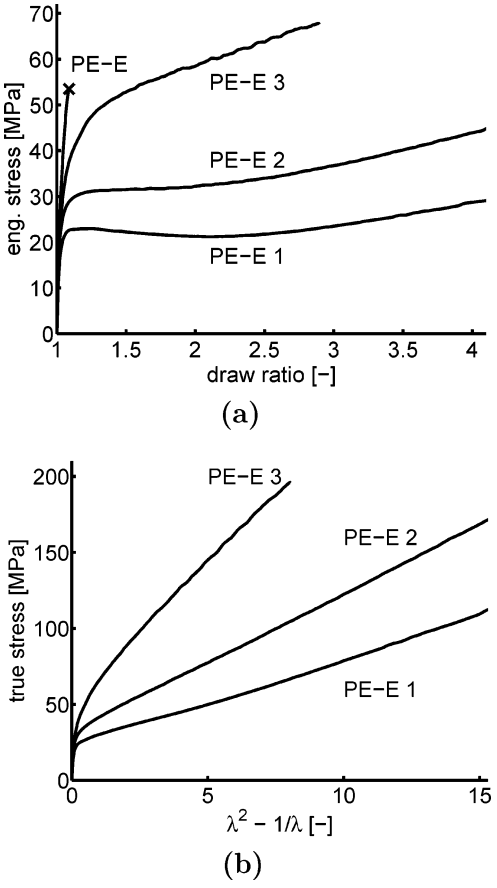

Figure 16. Macroscopic tensile behavior of injection-molded sample (PE-E) and extruded sheets of PE-E (1, 2, 3) tested in flow direction: (a) engineering stress−strain; (b) true stress−strain.

Table 6. Tensile Testing Results of Extruded PE

	PE-E 1	PE-E 2	PE-E 3
σ_y [MPa]	22	28	35
G_R [MPa]	6	9	18
σ_y/G_R	3.7	3.1	1.9

Table 7. Average *c*-Axis and Relative *A-Axis Orientations, $f_{c,av}$ and [A*]**

Injection			
	PP-I A	PP-I B	PP-I C
$f_{c,av}$	0.34	0.27	0.25
[A*]	0.5	0.6	0.7
Extrusion			
	PP-E 1	PP-E 2	
$f_{c,av}$	0.5	0.5	
[A*]	0.9	0.4	

Mechanical Properties of Polyethylene. It was shown previously[36] that deformation and failure of polymers can be described with a simplified model based

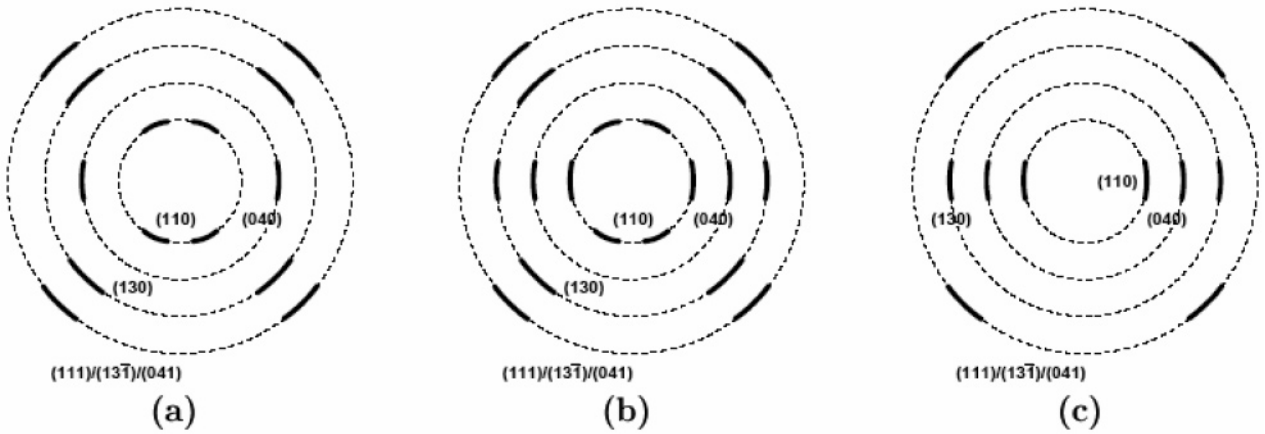

Figure 17. Schematic illustration of 2D-WAXD patterns of α-iPP, measured in this study. Flow direction was vertical. Orientation increases from dominant *a**-axis (a) to *c*-axis (c) orientation. (b) shows an intermediate pattern.

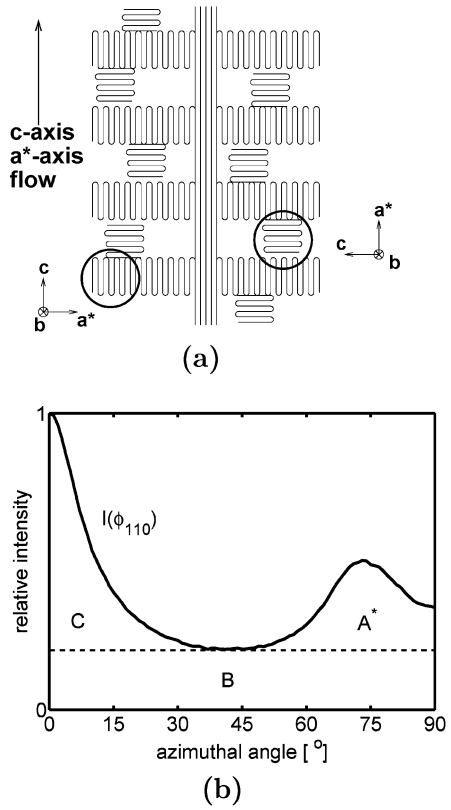

Figure 18. Lamellar branched shish-kebab structure (a) and method to determine fraction [A*] from (110) azimuthal scan curve. Both according to Fujiyama et al.[8,28] Flow direction is vertical in (a) and at 90° in (b).

on a stability analysis, yielding

$$\frac{\sigma_y}{G_R} = \frac{\lambda_n^{\,2} - (1/\lambda_n)}{\lambda_n - 1} \tag{11}$$

where σ_y and G_R are respectively the intrinsic yield stress and strain hardening modulus (from $\sigma_{true} = \sigma_y + G_R(\lambda^2 - 1/\lambda)$) and λ_n is the estimated "natural draw ratio" of the neck. Although it was shown that eq 11 is not in quantitative agreement with the materials' behavior, a qualitative relationship between σ_y/G_R and λ_n was found to be valid. Although the intrinsic behavior of the oriented polymer samples cannot be measured, e.g., with uniaxial compression tests, the macroscopic phenomena, like yield stress and "natural draw ratio", will be investigated and, if possible, results will be interpreted qualitatively.

Since the stress−strain curves of most injection-molded samples tested show similar behavior with respect to neck drawing, representative curves are plotted only in Figure 15. Results of yield stress and "natural draw ratio" of the injection-molded samples are summarized in Table 5. Figure 15a shows the behavior of the PE-I grade tested in flow direction. Necking starts in all samples at the position far from the gate, where the oriented skin layer was found to be smallest, and the neck grows in the direction of the gate. Apparently, the oriented structure increases the yield stress, and yielding starts for lowest orientation. This relation is also found when testing in perpendicular direction since for all molding conditions and materials, the yield stress decreases with increasing distance from the gate. Comparison of the yield stress in flow direction (starting far from the gate) with that in perpendicular direction at the similar position (PERP-3) shows the effect of anisotropy on yield stress. Since yield stress is considered to be related to lamellar thickness,[43] the differences in yield stress (in Figure 15a) are expected to be a result of the amount of shish present in the samples. The extended polymer chains which form a shish can be regarded as extremely thick lamellae, which possess a high yield stress. Sample PE-I C was shown to have a much lower orientation, giving a lower yield stress than samples PE-I A and B.

Strain hardening is also influenced by orientation as the "natural draw ratio" is found to be lowest upon testing in flow direction. Using the relation given in eq 11 and considering that the yield stress is increased in flow direction, the strain hardening modulus, G_R, is expected to be higher in flow direction. In sample PE-I A the influence of strain hardening, caused by the thick orientation layer, is evenly pronounced as the draw ratio in the neck, which decreases upon growing in the direction of the gate (see also the increase of stress upon drawing).

Sample PE-E A also shows an influence of the oriented layer thickness along the flow path when tested perpendicular to the machine direction (Figure 15), with respect to stability of deformation, as unstable or even brittle failure is observed when testing samples close to the injection gate. This can be rationalized to be a result of both a higher yield stress as a lower strain hardening (perpendicular to MD).

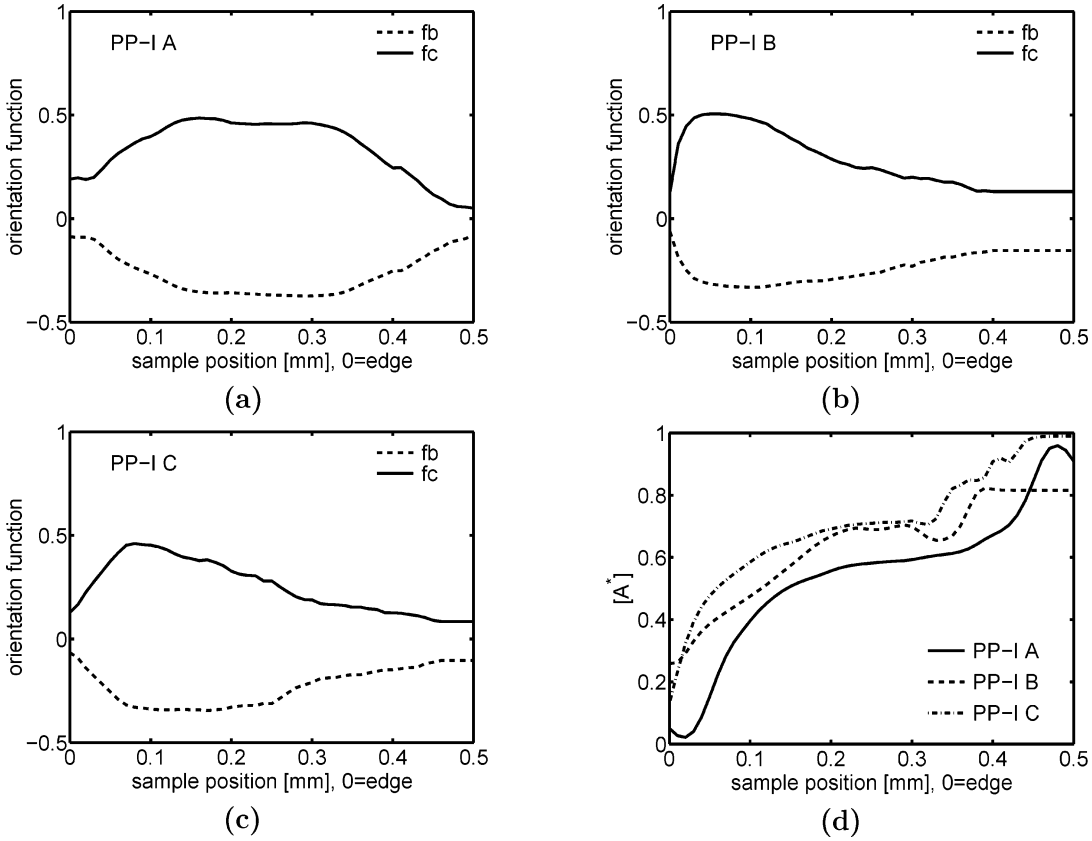

Figure 19. Orientation functions, f_b and f_c (a, b, c) and fraction [A*] (d) in flow over half the thickness of injection-molded samples of PP.

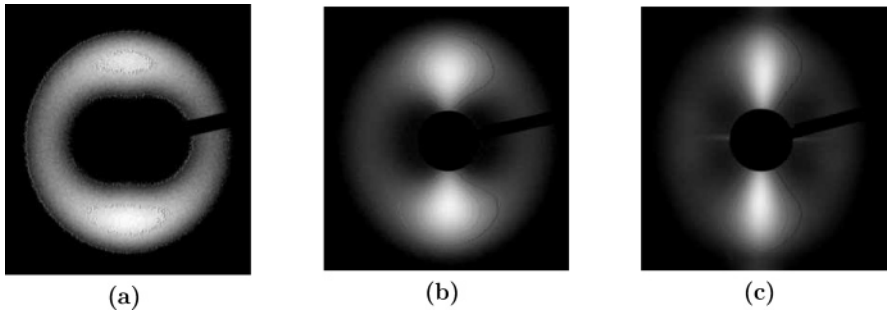

Figure 20. SAXS patterns of extruded PP-E samples, PP-E1 (a) and PP-E2 (b), and injection-molded PP-I sample (c) taken in ND direction with the beam going through the complete thickness. Flow is in vertical direction of images.

The influence of both yield and strain hardening is also illustrated in the impact toughness results, presented in Table 5. In previous work,[36] the intrinsic (isotropic, nonoriented) impact toughness for a grade PE-I was found to be on the order of 10 kJ/m^2. In its brittle failure mode the impact toughness was found to increase with intrinsic yield stress. Considering the impact toughness of the samples tested perpendicular to flow direction, a brittle−ductile transition is now found for a decreasing yield stress. Furthermore, impact testing in flow direction causes a brittle−ductile transition as a result of the increased strain hardening, yielding ultimate values of 16 times the intrinsic toughness for the sample with the strongest orientation.

The tensile behavior of the higher molecular weight grade, PE-E, is presented in Figure 16a. The extruded samples were only tested in flow direction, while the results of the injection-molded PE-E sample, tested in perpendicular direction, are given in Table 5. Similar to the results of the lower molecular weight grade, both yield stress and strain hardening are affected by orientation. However, the importance of the presence of highly oriented shish's on yield stress is emphasized, as the injection-molded sample fails in a brittle mode at a stress before yielding is initiated. The highly oriented extrusion sample (PE-E 3), on the other hand, does not fail at low strains and shows a homogeneous deformation before failure. This tendency to deform without necking is also observed in the lower oriented extrusion sheets, and taking a reduction in cross section to be proportional to the draw ratio, the true stress−strain curves are given in Figure 16b. Strain is plotted as $\lambda^2 - 1/\lambda$, such that the strain hardening modulus, G_R, can be determined. Results of yield stress and strain hardening modulus are reproduced in Table 6. In the case of the nonnecking samples, the yield stress was defined as the stress level at a strain of 7%, in the middle of the transition from the elastic to the strain hardening region. The ratio of yield stress and strain hardening drops down to values of 3 or lower, which is in agreement with neck drawing behavior according a stability analysis.[36] Sample PE-E 1 was also subjected

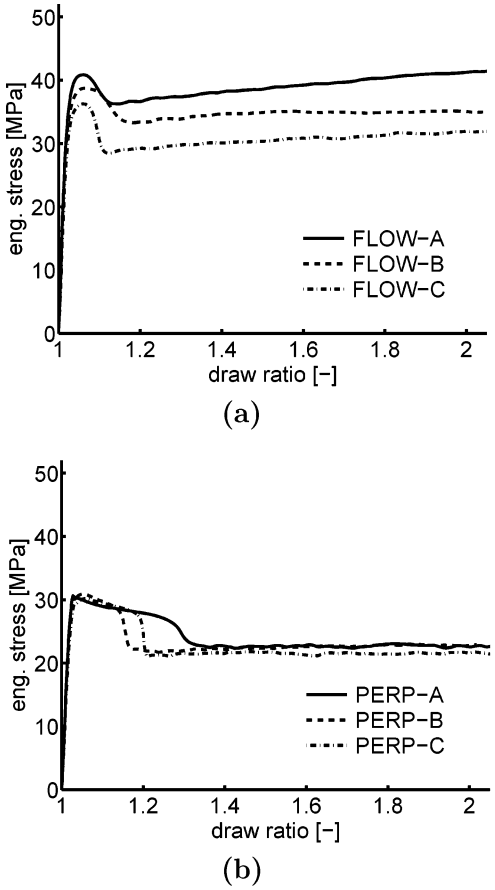

Figure 21. Macroscopic tensile behavior of injection-molded samples of PP-I, tested in flow (a) and perpendicular to flow direction (b), subjected to different molding conditions: (A) T_{inj} = 185 °C, Q_{inj} = 10 cm²/s; (B) T_{inj} = 185 °C, Q_{inj} = 100 cm²/s; (C) T_{inj} = 260 °C, Q_{inj} = 10 cm²/s.

Table 8. Tensile and Impact Testing Results of Injection-Molded PP Specimens

	σ_y [MPa]	Izod [kJ/m²]
	PP-I A	
FLOW	41	45
PERP	30	4
	PP-I B	
FLOW	39	25
PERP	30	5
	PP-I C	
FLOW	36	17
PERP	30	5

to impact testing and yielded an ultimate impact toughness of 380 kJ/m², which is approximately 6 times the intrinsic impact toughness of a nonoriented sample of this material.[36] The stronger oriented samples, PE-E 2 and 3, were not tested in impact since the thickness of these samples is below 1 mm, which is expected to change the stress state to a plain stress condition, influencing the notched impact behavior.

WAXD of Polypropylene. The WAXD images taken from the different positions along the thickness of the polypropylene samples show typical patterns as schematically illustrated in Figure 17. In total, three Debye rings of unique crystal reflections are visible ((110), (040), and (130)) and one of three interfering reflections ((111), (13$\bar{1}$), and (041)). These reflections all originate from an α crystalline phase, since no γ phase was found. In contrast to the work of Zipper et al.,[4,5] only a very weak β phase was observed in highly oriented structures, which will therefore not be taken into account in this study. Differences between these patterns are observed in the (110) and (130) reflections and were explained by Fujiyama et al.[8] as follows: when orientation is strong, the morphology is composed of shish-kebabs in which *c*-axis orientation dominates in flow direction, resulting in pattern (c). On the oriented lamellae (kebabs), epitaxial crystallization causes the growth of secondary lamellae of which the chains are perpendicular to the chain axis of the primary component (see Figure 18a). This orientation, which is also known as lamellar branching, causes an a^*-axis orientation in flow.

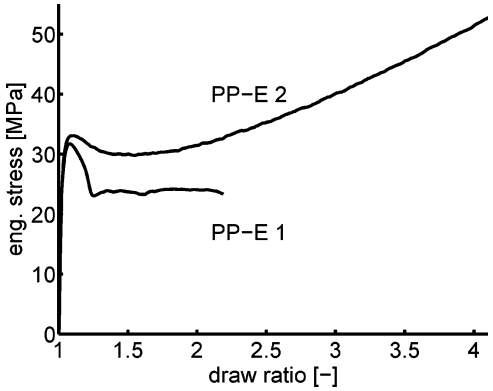

Figure 22. Tensile testing results of extruded PP-E.

A relative comparison between *c*-axis and a^*-axis orientation can be made from calculation of the fraction of a^*-axis component, [A*], which can be evaluated from the azimuthal scan curve of the (110) reflection according to Fujiyama's method:[8]

$$[A^*] = \frac{A^*}{C + A^*} \tag{12}$$

where *C* is taken as the area around an azimuthal angle of 0° and A^* the area around 90°, after subtraction of the baseline area *B* (see Figure 18b).

The WAXD results of the oriented layers in the injection-molded samples showed strong oriented patterns. Therefore, rotational symmetry of the shish-kebab structures was assumed, and the f_c and f_b orientation functions were calculated according to eqs 5 and 6 with

$$\langle \cos^2 \epsilon \rangle = \langle \cos^2 \phi_{040} \rangle \tag{13}$$

$$\langle \cos^2 \sigma \rangle = 1 - 0.901 \langle \cos^2 \phi_{040} \rangle - 1.099 \langle \cos^2 \phi_{110} \rangle \tag{14}$$

where $\langle \cos^2 \sigma \rangle$ is calculated using Wilchinsky's method[42] from the (110) and (040) reflections and the angle of 72.5° between the *b*-axis and the (110) plane. Figure 19 gives the distribution of the orientation functions in flow direction over half the thickness of the injection-molded samples. The oriented layer shows values of f_c of approximately 0.5, which are in the same order as found by Lamberti et al.[35] from FT-IR measurements on similar samples. Thicknesses of the oriented layers can be compared with the ones observed form optical micrographs (Figure 6).

The fraction [A*] is found to be almost zero at the outer skin, where the cooling rate is highest and secondary nucleation is not possible. The majority of the oriented layer, however, shows a fair amount of lamellar branching, whereas in the core a^*-axis orientation seems to dominate. To give an indication in different

orientation levels of the injection-molded samples, the average values, $f_{c,av}$ and $[A_a^* v]$, are given in Table 7.

Scanning of the extruded samples gave uniform results along the thickness, and their average values are summarized in Table 7. The main difference in the extruded samples is found in [A*], and the value of 0.9 that is found in sample PP-E 1 suggests a completely different orientation than that of sample PP-E 2. Next, using results of small-angle X-ray scattering, we will give a more detailed investigation of the differences in lamellae orientation.

SAXS of PP Samples. Figure 20 shows the SAXS images of samples PP-E 1, PP-E 2, and PP-I A. The first image shows that only a small amount of lamellae oriented perpendicular to flow is observed in the low elongated extrusion sample, whereas increasing the draw ratio (sample PP-E 2, image b) increases this lamellae orientation as seen from the intensity spots at the meridian. The last image, which is typically for all injection-molded PP-I samples, again shows the intensity spots at the meridian caused by oriented lamellae. Similar to what was observed in the SAXS patterns of injection-molded PE, a streak in equatorial direction is visible near the beamstop, indicating the existence of a reasonable amount of shish. Furthermore, the lamellar halo also shows small intensity spots at the equator, which is an evidence for lamellar branching. The SAXS patterns shown in Figure 20 also compare well to those found by Zipper et al.[4] on skin and core regions of injection-molded polypropylene.

Mechanical Properties of PP Samples. The engineering stress−strain curves of the injection-molded polypropylene samples tested in flow and perpendicular to flow direction are given in Figure 21. The observed trends in yield stress and strain hardening are similar to the ones observed in polyethylene: an increase in yield stress and strain hardening upon orientation in flow direction. Yield stress is considered to be increased by the formation of extended crystals (shish) and strain hardening, causing a decrease in natural draw ratio (Table 5), mainly due to the orientation of lamellae (kebabs). Loading in perpendicular direction shows no considerable differences for all samples produced and also not for the different positions along the flow path. Testing in perpendicular direction causes craze formation, accompanied by localization and macroscopic yield, in the oriented skin layer.

The impact toughness (see Table 8) is again found to be highest in orientation direction and related to the degree of orientation. The intrinsic impact toughness of a nonoriented sample of the PP-I grade is ∼10 kJ/m^2, so a maximum increase by a factor of 4.5 was found.

Tensile tests of the extruded samples of PP-E are presented in Figure 22. Here, the yield stress is found to be lower compared to the injection-molded samples, which indicates a lower amount of extended crystals (shish) as already observed from the SAXS patterns. Localization of the elongated sample PP-E 2 is, however, almost absent, which again proves the effect of oriented lamellae on the increase of strain hardening.

Conclusions

Flow-induced oriented structures in injection-molded and extrusion-casted polyethylene and polypropylene samples were charactarized by optical microscopy, X-ray scattering techniques, and transmission electron microscopy. The optical micrographs show layers of different level of orientation. Layer thickness in injection-molded samples is found to decrease along the flow path and increase for lower melt temperatures and longer filling times. Wide-angle X-ray diffraction patterns taken along the thickness of the sample indicate the existence of several layers, composed of orientation varying from lamellae row structures to highly oriented shish-kebabs. These textures were confirmed by small-angle X-ray scattering and transmission electron microscopy images. Since the extruded samples did not show a significant variation of orientation along the thickness, pole figures were measured by rotation of the samples along machine direction. Orientation of these samples was found to be dominated by a row structure. For indication of the average level of orientation, Hermans' orientation functions were either calculated from the flat plate WAXD patterns or from the pole figure results. Most of these characterization techniques were also applied to the polypropylene samples, where lamellae orientation, shish-kebabs, and lamellar branching could be distinguished. From tensile tests, performed in and perpendicular to flow direction, the yield stress was found to increase in the flow direction due to the amount of oriented shish, whereas strain hardening was assumed to be mainly increased by chain orientation forming oriented lamellae (kebabs). Since the extruded samples showed low yield stresses and strong strain hardening, these samples tended to deform homogeneous or with a very low draw ratio in the neck. This increase in strain hardening, caused by the lamellae orientation, is also responsible for the observed ultimate impact energy in flow direction. This toughness enhancement is found to be less pronounced for the polypropylene samples.

Acknowledgment. The authors acknowledge Christian Riekel for the availability of the X-ray facilities at the Micro-focus beamline (ID13) at the European Synchrotron Radiation Facility (ESRF, Grenoble, France) and the financial support provided by the Dutch Polymer Institute (DPI) (project 164).

References and Notes

(1) Kantz, M. R.; Newman, H. D.; Stigale, F. H. *J. Appl. Polym. Sci.* **1972** *16*, 1249−60.
(2) Altendorfer, F.; Seitl, E. *Kunststoffe* **1986**, *76*, 47−50.
(3) Trotignon, J.-P.; Verdu, J. *J. Appl. Polym. Sci.* **1987**, *34*, 1−18.
(4) Zipper, P.; Jánosi, A.; Wrentschur, E.; Abuja, P. M. *J. Appl. Crystallogr.* **1991**, *24*, 702−8.
(5) Zipper, P.; Jánosi, A.; Geymayer, W.; Ingolic, E.; Fleischmann, E. *Polym. Eng. Sci.* **1996**, *36*, 467−82.
(6) Mencik, Z.; Fitchmun, D. R. *J. Polym. Sci., Polym. Phys. Ed.* **1973**, *11*, 973−89.
(7) Matsumoto, K.; Miura, I.; Hayashida, K. *Kobunshi Ronbunshu* **1979**, *36*, 401−6.
(8) Fujiyama, M.; Wakino, T.; Kawasaki, Y. *J. Appl. Polym. Sci.* **1988**, *35*, 29−49.
(9) Schrauwen, B. A. G.; Govaert, L. E.; Peters, G. W. M.; Meijer, H. E. H. *Macromol. Symp.* **2002**, *185*, 89−102.
(10) Hsiung, C. M.; Cakmak, M. *J. Appl. Polym. Sci.* **1993**, *47*, 125−47.
(11) Hsiung, C. M.; Cakmak, M. *J. Appl. Polym. Sci.* **1993**, *47*, 149−65.
(12) Ulcer, Y.; Cakmak, M.; Miao, J.; Hsiung, C. M. *J. Appl. Polym. Sci.* **1996**, *60*, 669−91.
(13) Ulcer, Y.; Cakmak, M. *Polymer* **1997**, *38*, 2907−23.
(14) Zuidema, H. Ph.D. Thesis, Eindhoven University of Technology, The Netherlands, 2000.
(15) Zuidema, H.; Peters, G. W. M.; Meijer, H. E. H. *Macromol. Theory Simul.* **2001**, *10*, 447−60.
(16) Kubát, J.; Møanson, J.-A.; Rigdahl, M. *Polym. Eng. Sci.* **1983**, *23*, 877−82.

(17) Kalay, G.; Sousa, R. A.; Reis, R. L.; Cunha, A. M.; Bevis, M. J. *J. Appl. Polym. Sci.* **1999**, *73*, 2473−83.
(18) Kech, A.; Ludwig, H.-C.; Möginger, B.; Eyerer, P.; deClaville Christiansen, J. *Int. Polym. Proc. XV* **2000**, *2*, 202−7.
(19) Peters, G. W. M.; Swartjes, F. H. M.; Meijer, H. E. H. *Macromol. Symp.* **2002**, *185*, 277−92.
(20) Jerschow, P.; Janeschitz-Kriegl, H. *Rheol. Acta* **1996**, *35*, 127−33.
(21) Keller, A.; Machin, M. J. *J. Macromol. Sci., Part B* **1967**, *1*, 41−91.
(22) Kalay, G.; Bevis, M. J. *J. Polym. Sci., Part B: Polym. Phys.* **1997**, *35*, 241−63.
(23) Kalay, G.; Bevis, M. J. *J. Polym. Sci., Part B: Polym. Phys.* **1997**, *35*, 265−91.
(24) Lindenmeyer, P. H.; Lustig, S. *J. Appl. Polym. Sci.* **1965**, *9*, 227−40.
(25) Guan, Q.; Shen, K.; Ji, J.; Zhu, J. *J. Appl. Polym. Sci.* **1995**, *55*, 1797−804.
(26) Ogbonna, C. I.; Kalay, G.; Allen, P. S.; Bevis, M. J. *J. Appl. Polym. Sci.* **1995**, *58*, 2131−35.
(27) Sweeney, J.; Duckett, R. A.; Ward, I. M. *Proc. R. Soc. London A* **1988**, *420*, 53−80.
(28) Fujiyama, M.; Wakino, T. *J. Appl. Polym. Sci.* **1991**, *43*, 57−81.
(29) Wenig, W.; Herzog, F. *J. Appl. Polym. Sci.* **1993**, *50*, 2163−71.
(30) Liu, G.; Zhu, P. W.; Edward, G. *Macromol. Symp.* **2002**, *185*, 327−40.
(31) Choi, D.; White, J. L. *Polym. Eng. Sci.* **2002**, *42*, 1642−56.
(32) Fleischmann, E.; Koppelmann, J. *Kunststoffe* **1987**, *77*, 405−8.
(33) Fleischmann, E.; Koppelmann, J. *Kunststoffe* **1988**, *78*, 453−5.
(34) Lamberti, G.; La Carrubba, V.; Piccarolo, S.; Brucato, V. *Polym. Bull. (Berlin)* **2003**, *50*, 413−20.
(35) Lamberti, G.; Peters, G. W. M.; Schrauwen, B. A. G. *Polym. Bull. (Berlin)* **2003**, *50*, 405−11.
(36) Schrauwen, B. A. G. PhD Thesis, Eindhoven University of Technology, 2003; Chapter 3, pp 25−47 (http://www.mate.tue.nl/mate/pdfs/2886.pdf). See also: van Melick, H. G. H.; Govaert, L. E.; Meijer H. E. H. *Polymer* **2003**, *44*, 3579−91.
(37) Montezinos, D.; Wells, B. G.; Burns, J. L. *J. Polym. Sci., Polym. Lett. Ed.* **1985**, *23*, 421−5.
(38) Wenk, H.-R.; Matthies, S.; Donovan, J.; Chateigner, D. *J. Appl. Crystallogr.* **1998**, *31*, 262−9.
(39) Béguelin, P.; Barbezat, M.; Kausch, H. H. *J. Phys. III* **1991**, *1*, 1867−80.
(40) Odell, J. A.; Grubb, D. T.; Keller, A. *Polymer* **1978**, *19*, 617−26.
(41) Keller, A.; Kolnaar, H. W. H. *Mater. Sci. Technol.* **1997**, *18*, 189−268.
(42) Wilchinsky, Z. W. *J. Appl. Phys.* **1960**, *31*, 1969−72.
(43) Schrauwen, B. A. G.; Govaert, L. E.; Meijer, H. E. H. *Macromolecules* **2004**, *37*, 6069−78.

MA048884K